Molecular Therapy
Oncology
Original Article

Drug repurposing screen targeting PARP identifies cytotoxic activity of efavirenz in high-grade serous ovarian cancer

Bayley Matthews,[1,2] Michelle Wong-Brown,[1,2] Dongli Liu,[3] Christine Yee,[4] Kristie-Ann Dickson,[4] Jennifer Schneider,[1,2] Saiful Islam,[5] Richard Head,[5] Jennifer H. Martin,[1,2] Caroline E. Ford,[3] Deborah J. Marsh,[4] and Nikola A. Bowden[1,2]

[1]Drug Repurposing and Medicines Research Program, Hunter Medical Research Institute, New Lambton Heights, NSW 2305, Australia; [2]School of Medicine and Public Health, University of Newcastle, Newcastle, NSW 2289, Australia; [3]Gynaecological Cancer Research Group, School of Clinical Medicine, Faculty of Medicine and Health, University of New South Wales, Sydney, NSW 2052, Australia; [4]Translational Oncology Group, School of Life Sciences, Faculty of Science, University of Technology Sydney, Ultimo, NSW 2007, Australia; [5]Drug Discovery and Development, Clinical and Health Sciences, University of South Australia, Adelaide, SA 5000, Australia

Drug repurposing has potential to improve outcomes for high-grade serous ovarian cancer (HGSOC). Repurposing drugs with PARP family binding activity may produce cytotoxic effects through the multiple mechanisms of PARP including DNA repair, cell-cycle regulation, and apoptosis. The aim of this study was to determine existing drugs that have PARP family binding activity and can be repurposed for treatment of HGSOC. *In silico* ligand-based virtual screening (BLAZE) was used to identify drugs with potential PARP-binding activity. The list was refined by dosing, known cytotoxicity, lipophilicity, teratogenicity, and side effects. The highest ranked drug, efavirenz, progressed to *in vitro* testing. Molecularly characterized HGSOC cell lines, 3D hydrogel-encapsulated models, and patient-derived organoid models were used to determine the IC_{50} for efavirenz, cell death, apoptosis, PARP1 enzyme expression, and activity in intact cancer cells following efavirenz treatment. The IC_{50} for efavirenz was 26.43–45.85 μM for cells in two dimensions; 27.81 μM–54.98 μM in three dimensions, and 14.52 μM–42.27 μM in HGSOC patient-derived organoids. Efavirenz decreased cell viability via inhibition of PARP; increased CHK2 and phosphor-RB; increased cell-cycle arrest via decreased CDK2; increased γH2AX, DNA damage, and apoptosis. The results of this study suggest that efavirenz may be a viable treatment for HGSOC.

INTRODUCTION

Ovarian cancer is the eighth most commonly diagnosed cancer and cause of cancer-related death in women worldwide, with an estimated 314,000 cases diagnosed and 207,000 patients dying of the disease annually.[1] High-grade serous ovarian cancer (HGSOC), the most common subtype of ovarian cancer, accounts for approximately 70%–80% of all ovarian cancer deaths.[2] This is predominantly due to disease recurrence and innate or acquired resistance to current therapies. Efforts to find new treatments are ongoing; however, traditional drug development requires approximately 12–16 years and an investment of US$1–2 billion to achieve market approval.[3] This lengthy development pipeline, while necessary for identifying innovative treatments, is not the only option for providing patients with timely access to efficacious, cost-effective therapy.

Drug repurposing is a method for identifying new uses for approved or investigational drugs that are outside the scope of the original intended or approved medical use.[4,5] The development of repurposed drugs is attractive, both in terms of the substantial cost efficiencies it offers in comparison to drug discovery, and because therapeutic advances and new drug options for patients with ovarian cancer have been far slower than for other cancers.

Drug repurposing reduces the time for drug development by using the existing knowledge of pharmacokinetics, pharmacodynamics, common and uncommon toxicities, dosing schedule, and mechanism of action. As a result, most steps of the preclinical and early clinical development phases can be bypassed for repurposing drug candidates.[4] Drug repurposing also presents a significantly faster pathway into phase 2 trials in comparison to traditional drug discovery and development. This substantially reduces the development-related financial investment required.[5] In contrast to traditional drug discovery, repurposing a drug on average takes only 6.5 years to obtain approval and investment of US$300 million.[6]

Poly (ADP-ribose) polymerases (PARP) are a family of proteins that play key roles in DNA repair, chromatin remodeling, and maintaining genomic integrity.[7,8] There are 18 members of the PARP family, with the most well characterized member, PARP1, regulating the

Received 28 August 2024; accepted 21 November 2024;
https://doi.org/10.1016/j.omton.2024.200911.

Correspondence: Nikola A. Bowden, Drug Repurposing and Medicines Research Program, Hunter Medical Research Institute, New Lambton Heights, NSW 2305, Australia.
E-mail: nikola.bowden@newcastle.edu.au

DNA repair process through detecting and repairing single-strand DNA breaks (SSBs).[7,8] Because SSBs are produced during the base excision repair process, PARP1 is considered to be a vital part of this DNA repair pathway.[8] However, PARP1 is also involved in several alternate DNA repair pathways, including the homologous recombination (HR) pathway.[9] PARP2 and PARP3 have also been shown to have similar roles to PARP1 in DNA repair.[8]

Small molecule PARP inhibitors have been reported as effective first-line and maintenance therapy for ovarian cancer (reviewed in Zheng et al.[7,8]). These drugs act based on the concept of "synthetic lethality."[10,11] Inhibition of PARP repairing SSBs results in the formation of double-strand breaks (DSBs) during DNA replication, which would usually be repaired by the HR pathway.[10] Cancers containing *BRCA* mutations are HR-deficient (HRD), meaning that any DSBs that occur in these cells cannot be repaired through HR, resulting in an accumulation of DSBs leading to cell death.[10] As non-cancerous cells remain HR-proficient, they are able to repair DSBs and survive.[10] Therefore, PARP inhibitors selectively target cancer cells with DNA repair deficiencies, such as HRD.

The PARP family is involved in additional biological processes outside of DNA repair, including cell-cycle regulation and initiating apoptosis.[12,13] There remains unmet potential for targeting PARP more broadly via alternative approaches to small molecule inhibitors. Compounds with broad-spectrum PARP family binding activity could potentially produce cytotoxic effects through these multiple mechanisms of PARP. The aim of this study was to determine whether any existing drugs have broad-spectrum PARP family binding activity and could therefore be repurposed as a treatment for HGSOC. We hypothesized that targeting PARP for drug repurposing would elicit cytotoxic responses in HGSOC through multiple mechanisms including DNA repair, cell-cycle regulation, and apoptosis.

RESULTS

Potential PARP-binding activity for efavirenz

BLAZE software (Cresset Discovery Services, UK) *in silico* screening and filtering based on two commercial databases, which include all approved drugs from the British Pharmacopoeia, was used to identify 84 drugs with potential for broad-spectrum PARP family binding activity (Table S3). This list of 84 drugs was refined through cross-referencing with the Broad Institute PRISM Repurposing Database. Of the 84 drugs predicted by BLAZE to have broad-spectrum PARP family binding potential, 17 had data available in the 8 HGSOC cell lines used throughout this study (Figure S1). As a comparison, data were also collected on average log(2) fold change in cell viability following treatment with three small molecule PARP inhibitors currently approved for use in ovarian cancer treatment: olaparib, rucaparib, and niraparib. This filtering step identified 11 drugs with a negative log(2) fold change in cell viability in HGSOC cell lines in the PRISM dataset. The 11 drugs progressed through our drug repurposing pipeline for further screening.

We further refined the list of 11 drugs with negative log(2) fold change to four lead drugs (Table 1) by searching for known cytotoxicity within the approved dosing window. Appropriate lipophilicity was determined using logP and teratogenicity was also considered when filtering the list of drugs. Finally, data from other indications were collated to determine safety and toxicity. Didanosine did not proceed to further testing primarily due to an unacceptable toxicity profile. From this analysis, the top two lead drugs with cytotoxic potential and low toxicity were efavirenz and ganciclovir. We further tested these two drugs *in vitro*.

Efavirenz has cytotoxic effects in *in vitro* models of HGSOC

Efavirenz, a non-nucleoside reverse transcriptase inhibitor that is approved for the treatment of HIV infection, and ganciclovir, an antiviral used to treat cytomegalovirus infection, were both predicted to have PARP-binding activity potential. To determine whether either of these drugs also had cytotoxic effects in HGSOC, eight molecularly characterized HGSOC cell lines were treated with increasing doses of efavirenz or ganciclovir to determine the dose at which cell viability was reduced to 50% (half maximal inhibitory concentration [IC_{50}] value).

Ganciclovir doses were escalated up to 4 mM, but resulted in very limited changes in cell viability (data not shown). As the ganciclovir dose escalation was significantly higher than the reported maximum plasma concentration of the drug (12.2 μg/mL,[27] approximately 48 μM), it was determined to have low cytotoxicity potential and excluded from further screening. We continued *in vitro* testing of efavirenz as our lead candidate drug.

The HGSOC cell lines had mean IC_{50} values for efavirenz of 31.62 μM (range: 26.43–45.85 μM) (Figure 1). Surprisingly, no difference was found between IC_{50} values for homologous recombination deficient (HRD) *BRCA*-mutant (COV362, Kuramochi, OVSAHO; average IC_{50} = 29.59 μM) and homologous recombination proficient (HRP) *BRCA*-wild type (WT) (COV318, OAW28, OVCAR4, OVKATE, TYK-nu; average IC_{50} = 33.43 μM) cell lines.

We further tested the cytotoxic effects of efavirenz at similar doses to the minimum (26.43 μM), maximum (45.85 μM), and mean (31.62 μM) IC_{50} values. Doses of 25 μM, 35 μM, and 45 μM efavirenz were assessed using real-time live-cell analysis in three HGSOC cell lines chosen to be representative models of HGSOC: COV362 (*BRCA1* mutation), OVSAHO (*BRCA2* single copy deletion), and TYK-nu (WT *BRCA1/2*). After 7 days, significant differences were observed between vehicle and efavirenz-treated cells over time. Efavirenz significantly slowed cell growth, determined by cell count, in a dose-dependent manner in two (OVSAHO and TYK-nu) of the three cell lines tested (Figure 2A). Efavirenz also significantly induced cell death and apoptosis in a dose-dependent manner in all three cell lines tested (Figures 2B and 2C). The cell death and apoptosis induced by 45 μM efavirenz was similar to the levels induced by 30 μM carboplatin (platinum chemotherapy) and 17.5 μM Olaparib (PARPi) (Figures 2B and 2C), which are representative of the two main classes of standard of care treatment for HGSOC.

Table 1. Top four lead drug candidates with potential for broad-spectrum PARP family binding activity

	Didanosine	Efavirenz	Ganciclovir	Aminoglutethimide
Average log(2) fold change of cell viability	−0.354	−0.370	−0.092	−0.005
Original indication	HIV	HIV	Anti-viral	Anti-convulsant
Mode of delivery and dosing	Capsules 250–400 mg orally once daily	Capsules 600 mg orally once daily, in combination with a protease inhibitor and/or nucleoside reverse transcriptase inhibitors (FDA dosage)	5 mg/kg i.v. over 1 h, every 12 h (10 mg/kg/d) for 14 to 21 d	Capsules 250 mg orally every 6 h
logP	−0.869	4.457	−2.18	1.3
Half-life	0.8–1.9 h	40–55 h	2.5–6 h	12.5 h
Plasma C_{max}	2.2–11.8 μM	12.9–23.4 μM	47.8 μM	25.4 μM
Teratogenicity	Category B[a] Reproduction studies in rats and rabbits at doses up to 12–14.2 times the estimated human exposure (based on plasma levels) showed no evidence of impaired fertility or harm to the fetus. To be used during pregnancy only if the potential benefit justifies the potential risk.	Category D[b] Human data too limited to predict risk Embryotoxic (rats) Teratogenic (cynomolgus monkeys) Crosses placenta easily (rats and rabbits) Pregnancy should be avoided	Category D[b] Embryotoxic (mice/rabbits) Teratogenic (rabbits) Carcinogenic and mutagenic (mice) Crosses placenta easily (rats/rabbits) Pregnancy should be avoided	Category D[b] Teratogenic effects, including pseudohermaphroditism (rats) Carcinogenic (rats)
Pharmacokinetics	Rapidly absorbed after oral administration Peak Figure 6 concentrations observed from 0.25 to 1.5 h Binding to plasma proteins *in vitro* was low (<5%) Metabolized by the same pathways responsible for the elimination of endogenous purines	Well absorbed after oral administration Peak concentrations attained by 5 h Steady-state plasma concentrations reached in 6–10 d ∼99% of drug is plasma protein bound Nearly all urinary excretion is in the form of metabolites	Absorption of the oral form is very limited—about 5% fasting, about 8% with food ∼90% of drug in plasma eliminated unchanged in the urine	Rapid and complete absorption after oral administration ∼50% of drug eliminated in urine ∼50% of drug metabolized in liver mainly to *N*-acetylaminoglutethimide, hydroxylaminoglutethimine, and two minor metabolites, *p*-nitroglutethimide and formylaminoglutethimide
Cytotoxicity	N/A	Lung cancer,[14,15] leukemia,[16] breast cancer,[17–19] pancreatic cancer,[20,21] glioblastoma,[22] ovarian cancer,[23] prostate cancer[24]	N/A	Breast cancer[25]
Stroke and myocardial infarction	No evidence of increased CV events[26]	No evidence of increased CV events	Rare side effect	N/A

[a]Category B: Drugs that have been taken by only a limited number of pregnant women and women of childbearing age, without an increase in the frequency of malformation or other direct or indirect harmful effects on the human fetus having been observed.
[b]Category D: Drugs that have caused, are suspected to have caused, or may be expected to cause an increased incidence of human fetal malformations or irreversible damage.

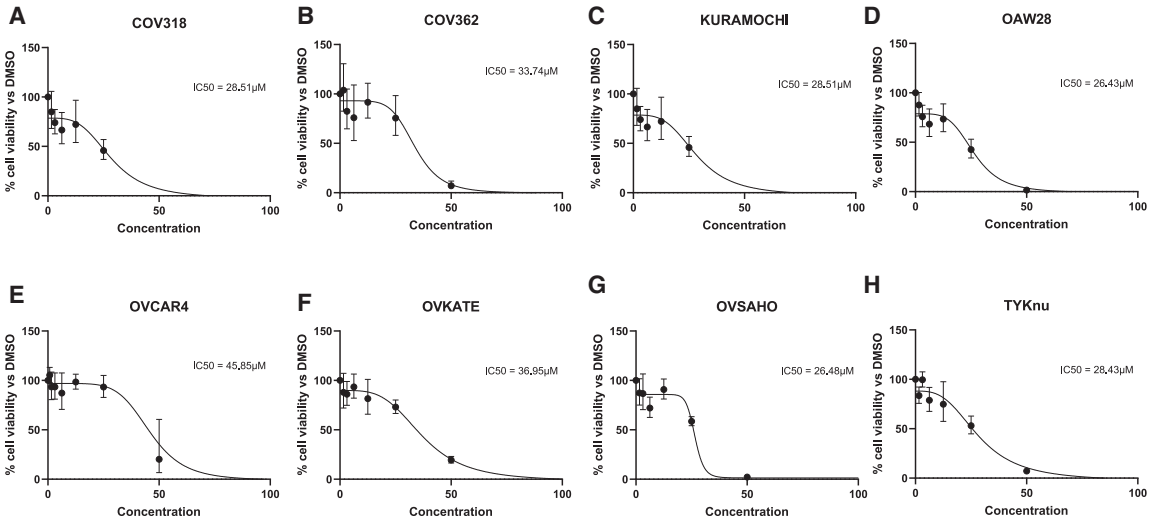

Figure 1. Inhibition IC_{50} values (μM) for efavirenz in HGSOC cell lines

HGSOC cell lines (A) COV318, (B) COV362, (C) KURAMOCHI, (D) OAW28, (E) OVCAR4, (F) OVKATE, (G) OVSAHO, and (H) TYK-nu were treated with serial 2-fold dilutions of efavirenz (1.5625, 3.125, 6.25, 12.5, 25, 50, and 100 μM) or DMSO vehicle control for 72 h. Cell viability was assessed by MTT assay. Data displayed is mean ± SEM of triplicates of three independent experiments. A non-linear regression curve was fitted to the data using GraphPad Prism version 10 (GraphPad Software, San Diego, CA, USA), and IC_{50} concentrations were extrapolated.

Clonogenic cell survival assays were conducted to assess whether efavirenz treatment affected colony formation in the HGSOC cell lines COV362, OVSAHO, and TYK-nu. The survival fraction was determined for all three cell lines and LC_{50} levels were extrapolated (Figure 3). There were no clear differences in efavirenz median lethal concentration (LC_{50}) levels between cell lines—OVSAHO (25.28 μM, 95% CI 21.29 μM–27.72 μM), TYK-nu (23.05 μM, 95% CI 22.05 μM–23.99 μM), and COV362 (26.49 μM, 95% CI 23.72 μM–29.06 μM). TYK-nu cells were more responsive to efavirenz over the dose curve compared with COV362 and OVSAHO that had surviving fractions that reached 0.30 and 0.43, respectively, at the highest efavirenz concentration tested (40 μM). The plating efficiencies, i.e., the number of cells seeded per well/number of colonies counted, in DMSO vehicle control wells were comparable across all cell lines tested, specifically OVSAHO (0.20), TYK-nu (0.24), and COV362 (0.30).

Efavirenz reduces expression and activity of PARP in HGSOC cell lines

PARP activity assays were performed to determine whether PARP1 enzyme activity was inhibited following efavirenz treatment. At 72 h, PARP1 activity in the COV362 cell line was significantly reduced following 45 μM efavirenz treatment (mean = 52.5% activity), and non-significantly reduced after 25 μM and 35 μM efavirenz treatment (mean = 79.3% activity for both treatment doses) (Figure 4A). In the OVSAHO cell line, 25 μM efavirenz significantly reduced PARP1 activity (mean = 74.3% activity); however, higher doses saw non-significant reductions in PARP1 activity (mean = 94.7% following 35 μM treatment, 88.6% activity following 45 μM treatment) (Figure 4B). PARP1 activity was significantly reduced in the TYK-nu cell line following all three doses of efavirenz treatment (mean = 36.2% following 25 μM treatment, 45.8% following 35 μM treatment, 40.4% activity following 45 μM treatment) (Figure 4C).

As PARP is also known to play a role in cell-cycle regulation,[12,13] the effect of efavirenz on cell-cycle progression was investigated using flow cytometry. In the three tested cell lines, efavirenz treatment (35 μM and 45 μM) increased the percentage of cells in the G1 phase, indicating its ability to arrest cells in the G1 phase. At these concentrations, there was a slight increase in the sub-G1 population, suggesting the induction of cell death (Figures 4D–4F).

Western blots were conducted to determine protein expression of both PARP1 and PARP2 in HGSOC cell lines following efavirenz treatment, along with expression of other downstream DNA damage (γ-H2AX), cell-cycle proteins (CDK2, phosphor-RB), and the housekeeping protein GAPDH. No significant differences were seen in PARP1 levels following treatment with a dose course of efavirenz over 48 or 72 h (Figures 5A–5D). However, PARP2 levels were shown to significantly decrease over an efavirenz dose course at 72 h in OVSAHO and TYK-nu cells, while showing a non-significant trend of reduced levels at 48 h in all cell lines tested (Figures 5A–5C and 5E). A marker of DSBs, γH2AX, was shown to significantly increase over the efavirenz dose course at 72 h in OVSAHO, with non-significant trends of increasing levels at other time points and cell lines with the exception of TYK-nu at 72 h (Figures 5A–5C and 5F). CDK2 controls G1/S transition and G2 progression through the cell cycle, as well as phosphorylates RB to induce S-phase entry.[28] Here, we show that efavirenz significantly decreased CDK2 levels with increasing doses at both 48 and 72 h in all cell lines tested (Figures 5A–5C and 5G).

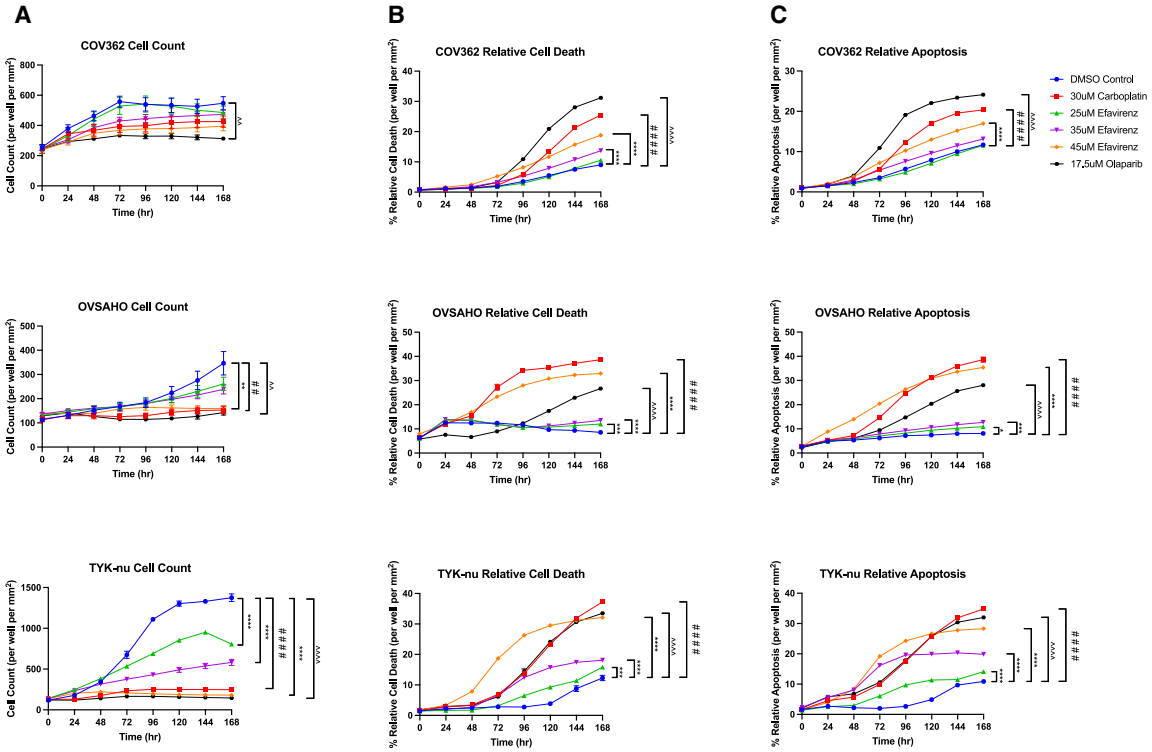

Figure 2. Efavirenz reduces cell confluence and induces cell death and apoptosis in a dose-dependent manner

HGSOC cell lines COV362, OVSAHO, and TYK-nu were treated with efavirenz (25 μM, 35 μM, or 45 μM), carboplatin (30 μM), or olaparib (17.5 μM) for 7 days. (A) cell count, (B) cell death, and (C) apoptosis were determined by real-time IncuCyte live-cell fluorescent assays. Data displayed is mean ± SEM of triplicates of three independent experiments. $^{*}p < 0.05$, $^{**}p < 0.01$, $^{***}p < 0.005$, $^{****}p < 0.001$ for efavirenz; $^{\wedge\wedge}p < 0.01$ and $^{\wedge\wedge\wedge\wedge}p < 0.001$ for Olaparib; and $^{\#\#}p < 0.01$ and $^{\#\#\#\#}p < 0.001$ for carboplatin, using one-way ANOVA at 168 h.

Efavirenz also significantly decreased phosphorylated RB in OVSAHO and TYK-nu cells over a dose course, as might be expected if the mechanism was decreased CDK2 that phosphorylated RB (Figures 5A–5C and 5H). RB could not be detected in COV362, consistent with previous reports that this cell line is null for RB.[29]

Efavirenz has cytotoxic effects in 3D models of HGSOC

To determine the effects of efavirenz in a more physiologically relevant model of HGSOC, three-dimensional (3D) hydrogel-encapsulated models for the cell lines COV362, OVSAHO, and TYK-nu were established. Dose-response curves to efavirenz were collected using 3D hydrogel-encapsulated models. The dose responses 72 h after addition of efavirenz were similar for TYK-nu, COV362, and OVSAHO cells and were less sensitive to efavirenz when cultured in 3D (Figure 6A) compared with 2D (Figure 1). The IC_{50} for efavirenz achieved in 2D models ranged between 26.43 and 45.85 μM, while that in 3D models ranged between 27.81 and 54.98 μM (Figure 6C). Interestingly, COV362 cells that have a clear *BRCA1* mutation displayed the highest resistance to efavirenz in WT3D models. Morphologically, at the dose most similar to the IC_{50} value for each cell line, a reduction in cell aggregation and 3D structure complexity within the hydrogel was observed, with complete cellular integrity loss at 100 μM efavirenz in all three cell lines (Figure 6B).

Efavirenz decreases ovarian cancer cell viability in patient-derived 3D organoid models

Finally, to determine the effect of efavirenz in a clinically relevant model of HGSOC, dose-response curves to efavirenz were collected for patient-derived 3D organoids. The patient-derived HGSOC organoids showed concordant expression patterns of relevant biomarkers (Figure S2). IC_{50} values for efavirenz in patient-derived organoids ranged from 14.52 to 42.27 μM (Figure 7A), which was a similar range to the 2D and 3D bioprinted models of HGSOC cell lines. The only organoid derived from a recurrent HGSOC case (OC005) showed the highest IC_{50} for efavirenz (42.27 μM). Compared with vehicle control, the patient-derived HGSOC organoids started to shrink in size following IC_{50} doses of efavirenz (Figure 7B).

In summary, efavirenz was determined to be a suitable candidate to repurpose for HGSOC treatment based on *in silico* screening and the drug's pharmacokinetic profile. *In vitro* testing found that efavirenz inhibited cell viability and induced cell death and apoptosis in multiple *in vitro* models of HGSOC, with similar IC_{50} values obtained between *BRCA*-mutant and *BRCA*-WT cell lines. No significant differences were seen in PARP1 expression in HGSOC cell lines following efavirenz treatment; however,

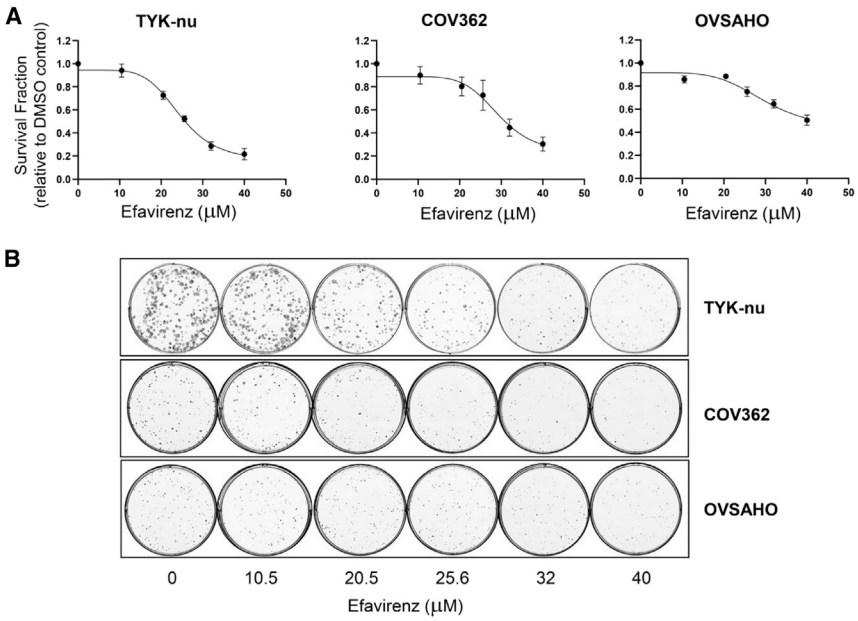

Figure 3. HGSOC cell survival clonogenic assays following treatment with efavirenz

Cell lines were treated with 0–40 μM concentrations of efavirenz. After 8 days (TYK-nu) or 14 days (COV362 and OVSAHO), colonies were fixed, stained with crystal violet, and counted on the GelCount instrument. Plating efficiency and survival fractions were determined and LC_{50} concentrations were extrapolated from (A) dose-response curves; Data displayed is mean ± SEM of four independent experiments. (B) Representative images of cell survival clonogenic assay.

PARP2 expression was significantly reduced in two cell lines tested. Additionally, efavirenz reduced enzymatic activity of PARP1 in HGSOC cell lines.

DISCUSSION

While most HGSOC patients initially respond to platinum-based chemotherapy, the majority will eventually become platinum-resistant with subsequent disease recurrences. The aim of this study was to identify drugs that could be rapidly repurposed to treat HGSOC through non-specific binding across the PARP family. After completing *in silico* screening using BLAZE (Cresset Discovery Services UK), 84 drugs were identified with potential for broad-spectrum PARP family binding activity. Further filtering using the Broad Institute PRISM dataset and *in silico* screening narrowed this list down to two lead drug candidates: efavirenz and ganciclovir. *In vitro* testing in eight HGSOC cell lines found that the IC_{50} values achieved for ganciclovir were markedly higher than the reported maximum plasma concentration of the drug (12.2 μg/mL).[27] Due to this, ganciclovir was excluded from our repurposing pipeline and *in vitro* testing continued with efavirenz.

Efavirenz is a non-nucleoside reverse transcriptase inhibitor (NNRTI) that received Food and Drug Administration (FDA) approval in 1998 for the treatment of HIV-1 infections.[30] Currently, efavirenz is most commonly used alongside two nucleoside reverse transcriptase inhibitors—emtricitabine and tenofovir—as a single-tablet triple antiretroviral therapy.[31] Efavirenz has several pharmacokinetic features that make it suitable to be repurposed as an anti-cancer drug, including its relatively long half-life (40–55 h) and average steady-state C_{max} of 12.9 μM.[32] Efavirenz is also well absorbed with oral administration, with peak plasma concentrations occurring 5 h following treatment.[32] Additionally, there is no evidence of efavirenz causing serious cardiovascular side effects such as stroke or myocardial infarction.[32]

Efavirenz was originally identified by BLAZE to have broad-spectrum PARP family binding potential. To date, there has only been one study investigating the effect of efavirenz on PARP. This study found that 10 μM efavirenz increased PARP activity, increased oxidative stress, and induced apoptosis and necrosis in normal endothelial cells.[33] No further studies have investigated the effect of efavirenz on PARP in cancer cells.

Due to efavirenz being predicted to have broad-spectrum PARP family binding potential, we originally hypothesized that efavirenz would inhibit the enzymatic activity of PARP and act in a similar manner to PARP inhibitors. However, several results from this study indicate that efavirenz does not act as a traditional PARP inhibitor. IC_{50} values obtained in 2D models were similar across eight HGSOC cell lines, with little difference between *BRCA*-mutant (COV362, Kuramochi, OVSAHO; average IC_{50} = 29.59 μM) and *BRCA*-WT (COV318, OAW28, OVCAR4, OVKATE, TYK-nu; average IC_{50} = 33.43 μM) cell lines. Additionally, the *BRCA2* mutant cell line COV362 had high IC_{50} values in both 2D (IC_{50} = 33.79 μM) and 3D (IC_{50} = 54.98 μM) models, and the BRCA-WT cell line TYK-nu had low IC_{50} values (2D IC_{50} = 28.43 μM, 3D IC_{50} = 27.81 μM). These results suggest that unlike PARP inhibitors, HR repair pathway deficiencies are not required in order to achieve a response with efavirenz treatment and would argue against a dominant influence of efavirenz on traditional PARP function.

Additionally, PARP inhibitors are highly potent molecules that bind specifically to the catalytic domain of PARP, with IC_{50} values for PARP enzyme inhibition in the nanomolar range. Olaparib has a PARP1 IC_{50} value of 5 nM and a PARP2 IC_{50} value of 1 nM, and is able to completely inhibit PARP1 activity at doses of 30–100 nM.[34,35] Similar results have been shown for other PARP inhibitors approved for use in ovarian cancer, such as rucaparib (PARP1 IC_{50} = 1.4 nM[34,36]) and niraparib (PARP1 IC_{50} = 3.8 nM, PARP2 IC_{50} = 2.1 nM[37]). However, not surprisingly efavirenz appears to inhibit PARP1 enzyme activity in intact cells at much higher doses.

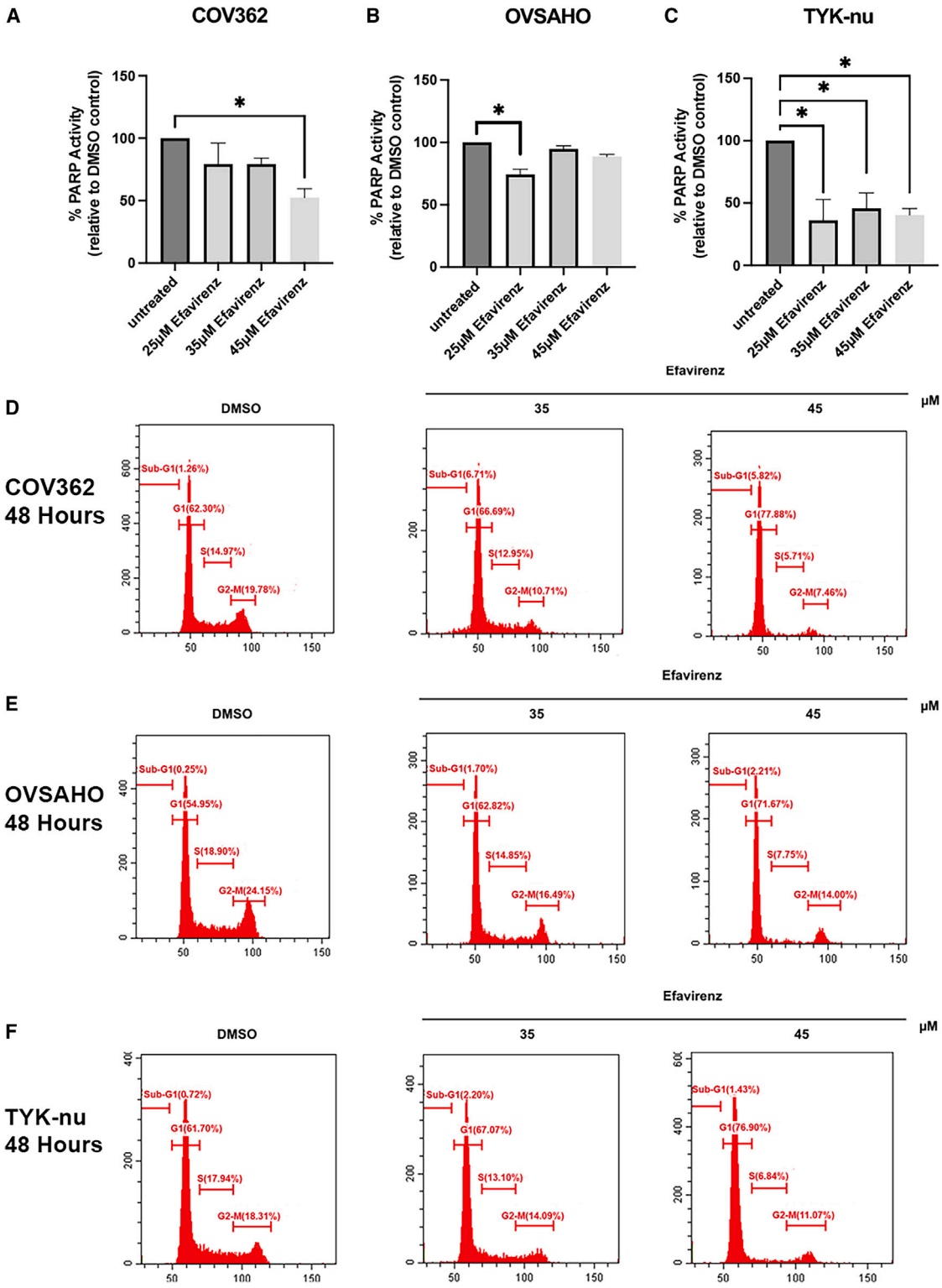

(legend on next page)

Both the COV362 and OVSAHO cell lines had reductions in PARP1 activity following 72 h efavirenz treatment at 45 μM (52.5% activity in COV362, 88.6% activity in OVSAHO), while PARP1 activity in TYK-nu was significantly reduced at a lower dose of 25 μM (36.2% activity). These results provide evidence that efavirenz may be partially acting through PARP enzyme inhibition.

Several *in vitro* studies have previously investigated the potential use of efavirenz as a treatment for many types of cancers, including lung cancer,[14,15] leukemia,[16] breast cancer,[17–19] pancreatic cancer,[20,21] glioblastoma,[22] ovarian cancer,[23] and prostate cancer.[24] However, the anti-cancer mechanism of action of efavirenz is still not understood. Several theories have been put forward to explain the cytotoxic effects of efavirenz, including interacting with the cannabinoid system[38] or estrogen receptors,[17] or targeting cancer stem cells.[18] However, the current leading hypothesis is that efavirenz selectively induces DNA damage and alters cell-cycle regulation in cancer cells. Plasma-level concentrations of efavirenz (13 μM) have been shown to activate several DNA damage response pathways, including the ATM and p53 signaling pathways,[14] as well as induce S-phase cell-cycle arrest[15] in *in vitro* studies of lung cancer. Similarly, 20 μM efavirenz treatment blocked progression of the cell cycle during G_0/G_1 phase and increased DNA damage in ovarian cancer cell lines.[23] Efavirenz has also been shown to induce apoptosis and increase expression of DNA damage markers p53, CHK2, and γH2AX phosphorylation in leukemia cell lines.[16]

The results from our study also support this theory of efavirenz inducing DNA damage and altering the cell cycle. γH2AX expression significantly increased after 72 h of efavirenz treatment in the OVSAHO cell line and trended toward increasing in COV362 and TYK-nu, suggesting an inhibition of DNA double-strand break repair following treatment with efavirenz. Both CDK2 and phosphorylated RB expression also decreased significantly in all cell lines and time points following efavirenz treatment, with the exception of COV362 for phosphorylated RB that is RB-null.[29] Additionally, 35-μM and 45-μM doses of efavirenz increased the percentage of cells in sub-G1 and G1 phases of the cell cycle in all three HGSOC cell lines tested, indicating that efavirenz induces cell-cycle arrest between G_1 and S phases, which supports similar results reported by Marima et al.[15] and Perna et al.[23] Efavirenz also induced apoptosis in all three HGSOC cell lines tested in a dose-dependent manner, which may have resulted from an accumulation of the effects of DNA damage within the cells following treatment with efavirenz. In summary, from the results of this study we proposed the mechanism of action of efavirenz in HGSOC is a decrease in cell viability via a combination of mild inhibition of PARP expression and activity in intact cancer cells, increased DNA damage, increased cell-cycle arrest, and increased apoptosis.

The results of this study suggest that efavirenz may be a viable treatment option for HGSOC independent of HR status. Efavirenz was identified through *in silico* ligand-based screening to have non-specific PARP family binding potential, and was determined to be a suitable candidate for repurposing based on several of the drug's pharmacological features and previous studies investigating the drug's cytotoxicity in various other cancer types. The toxicity profile of efavirenz was much lower than most other drugs identified during the *in silico* screen. The AIDS Clinical Trials Group 364 Study[39] and Study 006[40] reported treatment-related undesirable effects of at least moderate severity reported in at least 5% of patients were rash (11.6%), dizziness (8.5%), nausea (8.0%), headache (5.7%), and fatigue (5.5%). Nausea was reported with a higher frequency in the control groups. Severe neuropsychiatric symptoms occurred in 2.9% of the HIV population. These symptoms usually resolved within 4 weeks of commencing efavirenz (median duration 19 to 22 days) and patients with a past history of psychiatric conditions appear to be at higher risk.[39] To address this risk, history of neuropsychiatric conditions and close monitoring for psychological symptoms should be considered for inclusion in clinical trials to assess efavirenz in HGSOC.

In vitro testing of efavirenz found that clinically relevant doses of efavirenz inhibit cell viability and induce cell death and apoptosis in HGSOC cell lines, with similar IC_{50} values obtained between *BRCA*-mutant and *BRCA*-WT cell lines. Similar results were obtained in more physiologically relevant models of HGSOC, including 3D models and patient-derived organoids. Additionally, efavirenz was found to increase the percentage of cells stalled in the cell cycle and reduced activity of PARP1 in intact HGSOC cell lines, although not to the same extent as traditional PARP inhibitors. Investigations to determine the binding affinity of efavirenz to PARP are required to further explore the cytotoxic mechanism of action of efavirenz in HGSOC and its future potential use in treatment of HGSOC.

MATERIALS AND METHODS

In silico drug target analysis

Compounds with potential for broad-spectrum PARP family binding activity were identified using the *in silico* BLAZE application developed by Cresset Discovery Services UK.[41] BLAZE is a ligand-based virtual screening platform that uses the shape and electrostatic character of ligands to rapidly search large chemical collections for molecules with similar properties. This method generated a preliminary list of compounds that included approved and investigational drugs. An *in silico* search against the British Pharmacopoeia was conducted to identify compounds that had US FDA, European Medicines Agency (EMA), or Australian Therapeutic Goods Administration (TGA) approval for use in any indication.

Figure 4. Efavirenz inhibits PARP1 enzyme activity and cell cycle in HGSOC cell lines

HGSOC cell lines (A) COV362, (B) OVSAHO, and (C) TYK-NU were treated with efavirenz (25 μM, 35 μM, or 45 μM) for 72 h. PARP1 activity was measured using a PARP Activity Assay, with absorbance values expressed as a percentage of DMSO vehicle control values. Data displayed is mean ± SEM of triplicates. $^*p < 0.05$ using one-way ANOVA. HGSOC cell lines (D) COV362, (E) OVSAHO, and (F) TYK-NU were treated with efavirenz (35 μM or 45 μM) for 48 h. Cell cycle (Sub-G1, G1, S and G2) was collected as a percentage of total cell count.

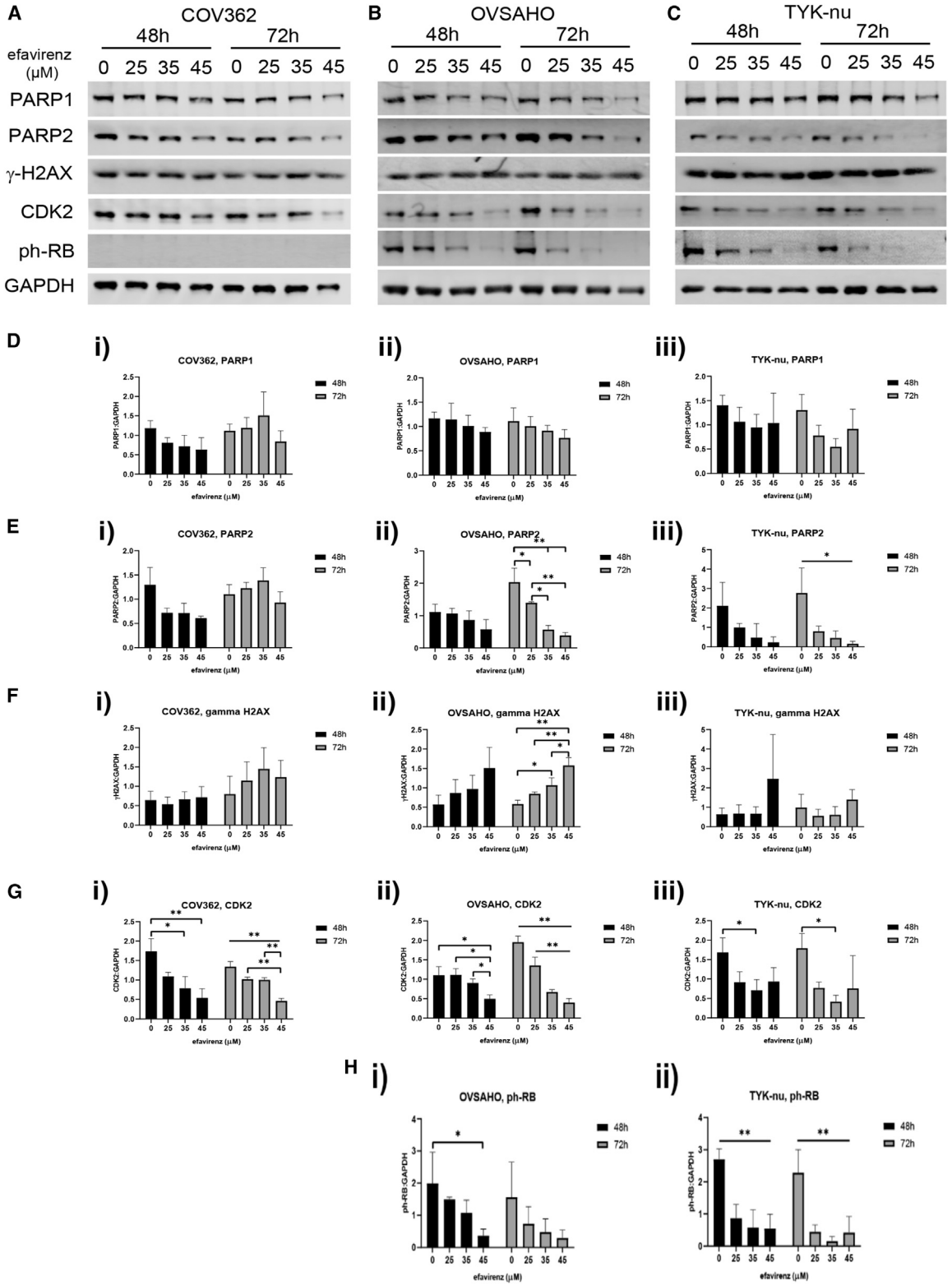

(legend on next page)

Drugs identified during the Cresset screen were cross-referenced with the Broad Institute PRISM Repurposing Database (https://depmap.org/repurposing/).[42] Briefly, the PRISM Repurposing 19Q3 Primary Screen involved cancer cell lines labeled with unique DNA "barcode" sequences being treated with a single dose (2.5 μM) of 4,518 compounds. After 5 days, the relative abundance of mRNA barcodes was measured as a surrogate for cell viability compared with vehicle control (DMSO)-treated cell lines.[42] Data from the Primary Screen Replicate Collapsed Logfold Change dataset was used to determine the average log(2) fold change in cell viability across eight HGSOC cell lines (KURAMOCHI, OVSAHO, COV362, OVCAR4, COV318, TYK-nu, OVKATE, and OAW28) following 2.5-μM treatment with drugs identified in the initial Cresset screen. Drugs with a negative average log(2) fold change compared with DMSO vehicle control were filtered for further screening.

This list of approved drugs with potential to bind to the PARP family with a negative log(2) fold change was then further filtered using *in silico* advanced screening. Literature searches were conducted to determine dosing, toxicities, method of delivery (using data from PubMed, Micromedex, and MIMS), lipophilicity (PubChem), teratogenicity (Briggs/MIMS/AUSDI), and cytotoxicity (PubMed). Drugs were ranked based on these criteria, with drugs that had lower doses, minimal toxicities, relevant delivery modes (e.g., oral delivery), and previous proof of anti-cancer activity ranking higher. The two highest ranked drugs progressed to *in vitro* testing.

Reduce, replace, refine statement

Reduce, Replace, Refine (RRR) the use of animals in research legislation encourages the use of advanced *in vitro* models to assess drug efficacy when safety and toxicity profiles are well established and subsequent animal experiments are not a requirement for FDA approval. Here, we describe three *in vitro* methods used to determine efficacy of efavirenz in HGSOC, including 2D cell lines, 3D bioprinted cell lines, and clinically relevant patient-derived 3D organoids, collected from HGSOC patients for the purposes of this study. Human Research Ethics approval for the study protocol and patient information and consent form were obtained from the South Eastern Sydney Local Health District Human Research Ethics Committee (SESLHD HREC, reference # 2021/ETH11975 and 19/001).

In vitro screening—2D HGSOC cell lines

Eight HGSOC cell lines were used in this study: KURAMOCHI, OVSAHO, COV362, OVCAR4, COV318, TYK-nu, OVKATE, and OAW28. These cell lines were confirmed by genomic and proteomic profiling to be representative of HGSOC.[29] The *BRCA* and *TP53* status of each cell line has previously been described.[29,43]

Three cell lines were selected for further testing as representative models of HGSOC: TYK-nu[29] (wild-type *BRCA1/2*; cat. #JCRB0234.0, Japanese Cell Resource Bank [JCRB]), COV362[44] (*BRCA1* c.2611_2612ins1 [p.P871fs], and c.4095 + 1 G>T; cat. #07071910, European Collection of Authenticated Cell Cultures [ECACC]) and OVSAHO (*BRCA2* single copy deletion; cat. #JCRB1046, JCRB, Figure S3). All cell lines were distributed by CellBank Australia (Westmead, New South Wales, Australia).

Cells were cultured in either RPMI1640 (cat. #42402016, Thermo Fisher Scientific, Mulgrave, VIC, Australia) plus 10% fetal bovine serum (FBS; cat. #SFBS-AU, AusGeneX, Molendinar, QLD, Australia) (OVSAHO) or DMEM (cat. # 11965118, Thermo Fisher Scientific, Mulgrave, VIC, Australia) plus 10% FBS (COV362) or EMEM (cat. #11095098, Thermo Fisher Scientific, Mulgrave, VIC, Australia) (TYK-nu) plus 10% FBS at 37°C in a humidified 5% CO_2 atmosphere. Cell line authentication was undertaken by the Australian Genome Research Facility (AGRF) (Melbourne, Australia) as previously described.[45] Mycoplasma testing was conducted using the MycoAlert Mycoplasma Detection Kit (cat. #LT07-318, LONZA, Walkersville, MD, USA).

In vitro screening—3D bioprinted HGSOC cell lines

3D *in vitro* HGSOC models were created using the RASTRUM 3D bioprinter (Inventia Life Science, Sydney, Australia), using the proprietary PEG-based bioinks with tripeptide arginine-glycine-aspartic acid (RGD) biofunctionalization and 3 kPa stiffness (Px03.03P; Inventia Life Sciences). COV362, OVSAHO, and TYK-nu cells were bioprinted as a "large plug" model at a cell density of 6.25×10^6 cells/mL encapsulated in the biofunctionalized hydrogel on top of an inert hydrogel base in 96-well tissue culture treated, low evaporation plates (cat. #CLS3595, Sigma-Aldrich Pty. Ltd., Sydney, NSW, Australia). Bioprinted cells were allowed to form 3D structures for 5 days (TYK-nu) or 10 days (COV362 and OVSAHO) at 37°C and 5% CO_2 before addition of efavirenz or DMSO vehicle as per conditions for the determination of LC_{50} levels in 2D.

In vitro screening—Patient-derived 3D organoid model

Ovarian cancer tissue and ascites fluids were obtained from tumor resection, debulking, or drainage of ascites at the Royal Hospital for Women, Sydney, Australia. Ethics approval was obtained from the South Eastern Sydney Local Health District Human Research Committee (SESLHD HREC, reference # 2021/ETH11975 and 19/001). For the organoid culture, tissue samples were cut into small pieces

Figure 5. Protein levels of DNA damage and cell cycle proteins following treatment with efavirenz

Cell lines (A) COV362, (B) OVSAHO, and (C) TYK-nu were treated with 0, 25, 35, or 45 μM efavirenz for 48 or 72 h and underwent immunoblotting for PARP1, PARP2, γ-H2AX, CDK2, phosphor-RB, and GAPDH. Representative immunoblots are shown. Quantitative analyses were performed using data from three replicates relative to GAPDH, and then normalizing these data for each sample to a gel average. (D) PARP1 levels in i) COV362, ii) OVSAHO, and iii) TYK-nu. (E) PARP2 levels in i) COV362, ii) OVSAHO, and iii) TYK-nu. (F) γH2AX levels in i) COV362, ii) OVSAHO, and iii) TYK-nu. (G) CDK2 levels in i) COV362, ii) OVSAHO, and iii) TYK-nu. (H) Phosphor-RB levels in i) OVSAHO and ii) TYK-nu. COV362 is null for phosphor-RB. Data displayed is mean ± SEM of triplicates. Statistical analyses were performed using a one-way ANOVA with Tukey's post hoc test for multiple comparisons, $^*p < 0.05$, $^{**}p < 0.005$.

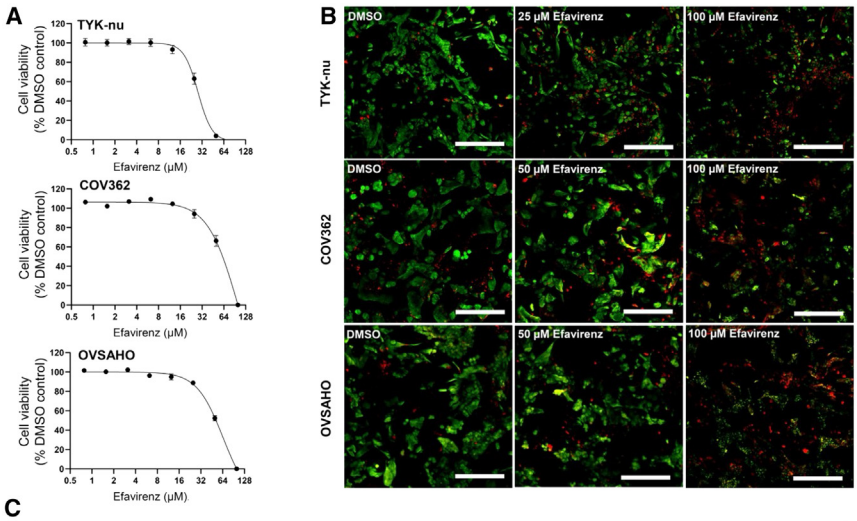

C

Cell Line	IC_{50} (μM)	95% CI (μM)
TYK-nu	27.81	26.31 - 29.59
COV362	54.98	n/a^ - 59.82
OVSAHO	49.82	47.11 – 52.44

Figure 6. HGSOC cell lines treated with efavirenz in 3D culture models

(A) Efavirenz dose response in TYK-nu, COV362, and OVSAHO in 3D cell cultures. Data displayed are mean ± SD of three independent experiments. (B) Representative maximum Z-projection images of LIVE/DEAD viability staining after 72 h efavirenz or DMSO vehicle control exposure in TYK-nu, COV362, and OVSAHO cell lines grown as 3D bioprinted models. Green = live, red = dead. Scale bar, 200 μm. (C) Cell viability (IC_{50} values) for bioprinted cell lines treated with efavirenz grown in 3D. IC_{50}, inhibitory concentration 50; CI, confidence interval; ^n/a, not available, unable to be determined.

and dissociated with collagenase IV (cat. # 17104019, Thermo Fisher Scientific, Mulgrave, VIC, Australia) and mechanical trituration. Clusters of tumor cells ("spheroids") were isolated from ascites fluid, as described previously.[46] Isolated cells were then embedded in 70% Matrigel/30% defined medium (cat. #356231, Corning, Glendale, AZ, USA) and cultured in the defined medium (Table S1). Organoids applied in the downstream analyses were processed and sectioned as formalin-fixed paraffin-embedded (FFPE) slides for histological confirmation of HGSOC markers by NSW Health Pathology diagnostic services. Hematoxylin and eosin (H&E) staining as well as immunohistochemistry (IHC) staining of HGSOC markers including p53 (Leica, DO7, 1:200), PAX8 (Biocare Medical, BC12, 1:100), and WT1 (Cell Marque, 6F-H2, 1:500) was performed in organoids and corresponding tumor tissue. Short-term passages of organoids (up to passage 2) were used in this study.

Efavirenz treatment

Stock solutions of efavirenz (HY-10572 MedChemExpress, NJ, USA) were dissolved in dimethyl sulfoxide (DMSO) at 100 mM and stored at −80°C. Efavirenz was further diluted in cell culture media to desired concentrations for use in treatments.

Cell viability assays

HGSOC cell lines were seeded into 96-well plates in triplicate wells and incubated for 24 h before treatment was added. The seeding densities of all cell lines were as follows: KURAMOCHI (4,000 cells/well); OVSAHO, COV318, and TYK-nu (3,000 cells/well); COV362 and OVKATE (5,000 cells/well); OVCAR4 and OAW28 (2,500 cells/well).

Serial 2-fold dilutions of efavirenz were performed to establish a dose-response curve from seven different concentrations (1.5625, 3.125, 6.25, 12.5, 25, 50, and 100 μM). The highest concentration of efavirenz used for the dose-response curve is 6.25 times higher than the maximum plasma concentration of efavirenz.[32]

The cells were treated with increasing concentrations of efavirenz or DMSO vehicle control for 72 h. After the 72-h treatment, cell viability was assessed using either MTT or MTS assay. For the MTT assay, MTT (cat. #M6494, Thermo Fisher Scientific, MA, USA) was added to a final concentration of 400 μg/mL. The cells were incubated for 3 h for the formation of formazan. The media containing the MTT was then removed, and the formazan crystals were solubilized in DMSO. The absorbance value of the dye was measured at 570 nm with a microplate reader (BMG LABTECH, Mornington, Victoria, Australia). Each experiment was performed in triplicate and repeated three times, with data reported as the mean ± SEM. The IC_{50} values (concentration of drug which causes 50% reduction in cell viability) were calculated using GraphPad Prism version 10 (GraphPad Software, San Diego, CA, USA). A non-linear regression curve was fitted to the data and IC_{50} concentrations were extrapolated.

For the MTS assay, cells were seeded into 96-well plates (COV362 5,000 cells/well; OVSAHO 5,000 cells/well; TYK-nu 2,500 cells/well), allowed to plate overnight, and treated with efavirenz (0.78–100 μM with 2-fold dilutions; cat. #HY-10572, MedChemExpress, Monmouth Junction, NJ, USA) or DMSO vehicle control (cat. #D2650, Sigma-Aldrich Pty. Ltd., Sydney, NSW, Australia) for 72 h before being assessed for cell viability using the CellTiter 96 AQueous One Solution Cell Proliferation Assay (cat. #G3581, Promega, Madison, USA). Each experiment was performed in triplicate and repeated three times, with data reported as the mean ± SEM. Relative lethal concentration 50 (LC_{50}) was calculated using GraphPad Prism version 9.4.1 for Windows (GraphPad Software, San Diego, CA, USA). A non-linear regression curve was fitted to the data and LC_{50} concentrations extrapolated.[47]

For 3D bioprinted cell lines and patient-derived organoids, cell viability was measured 72 h after the addition of efavirenz using the

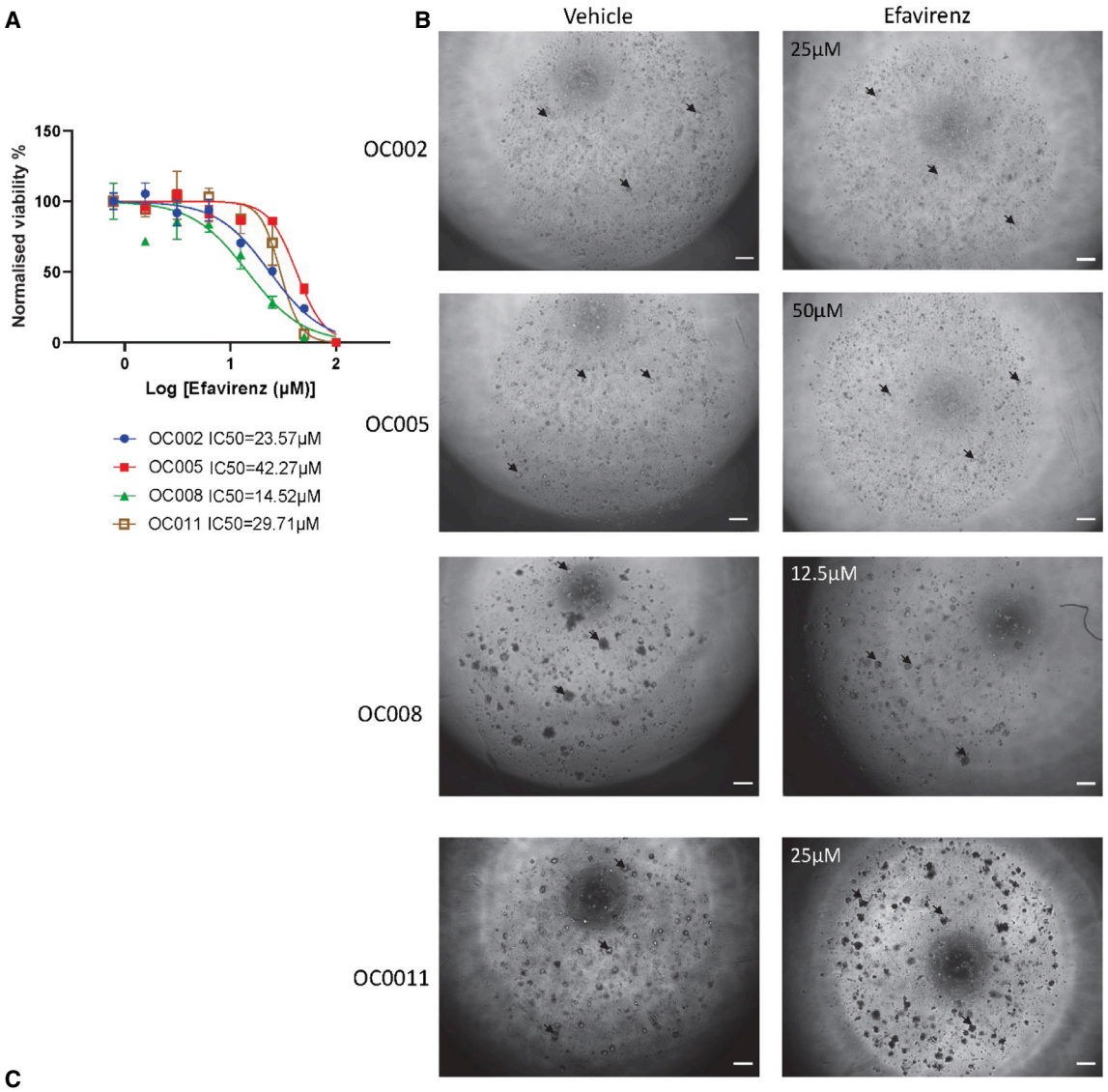

C

	Age	Diagnosis	BRCA Status	Treatment status at time of collection
OC002	49	HGSOC	gBRCA1 mutation	None
OC005	57	HGSOC Stage 1 (2011) Metastatic HGSOC (2022)	gBRCA1/2 wildtype	Carboplatin.paclitaxel in 2011
OC008	81	HGSOC Stage IIIC	gBRCA1/2 wildtype	6 weeks post-chemotherapy (6 cycles carboplatin and paclitaxel)
OC011	64	HGSOC Stage IIIC	Unknown	3 weeks post-chemotherapy (4 cycles of carboplatin and paclitaxel)

Figure 7. Ovarian cancer patient-derived 3D organoids treated with efavirenz

(A) Efavirenz dose response and estimated IC_{50} in four organoids. Error bars represent standard deviation for $n = 3$ technical replicates. (B) Representative images of organoids treated with efavirenz at the dose close to IC_{50} or DMSO vehicle control after 72 h. Arrows point out representative organoids. Scale bar, 200 μm. (C) Demographic and clinicopathological characteristics of patient-derived xenografts.

CellTiter-Glo-3D viability assay (cat. #G9681; Promega, Madison, USA) as per the manufacturer's instructions in triplicate wells repeated in three independent experiments. Cell viability with efavirenz treatment was expressed as a percentage of DMSO vehicle control and relative lethal concentration 50 (LC_{50}) values were calculated using a non-linear regression in GraphPad as described above.

To visualize the distribution of live and dead cells within the biofunctionalized hydrogel in response to efavirenz, *in situ* fluorescent viability staining using the LIVE/DEAD Viability/Cytotoxicity Kit for mammalian cells (cat. #L3224, Invitrogen, Thermo Fisher Scientific, Mulgrave, VIC, Australia) was performed. Briefly, media was removed and each well was washed twice with 1x phosphate-buffered saline. The kit's staining cocktail was prepared and added to each well as per the manufacturer's instructions for 30 min at 37°C protected from light. Wells were further washed with 1x phosphate-buffered saline prior to imaging and digital images were captured using a 10× objective on an STELLARIS confocal microscope (Leica Microsystems Pty. Ltd., Macquarie Park, NSW, Australia) at focal distances of 5μM combined to generate a composite image.

Live-cell imaging assays

Three HGSOC cell lines (COV362, OVSAHO, and TYK-nu) were seeded into 96-well plates (COV362 5,000 cells/well; OVSAHO 3,000 cells/well; TYK-nu 3,000 cells/well) in triplicate wells and incubated for 24 h. At 24 h, cells were treated with either DMSO vehicle control or the minimum, maximum, or mean IC_{50} dose of efavirenz obtained from the MTT assay (25 μM, 35 μM, and 45 μM). Cytotox Green (cat. #4633, Sartorius, Gottingen, Germany; final concentration of 2.5 nM) and Annexin Red (cat. #4641, Sartorius, Gottingen, Germany; final concentration of 1:400 of the reagent stock concentration) were also added at 24 h, as per manufacturer's protocol (Sartorius, Gottingen, Germany).

The wells were then imaged using the IncuCyte ZOOM high-throughput live-imaging system (Sartorius, Gottingen, Germany) at 10× objective using the green and red channels (triplicate wells per treatment condition, four images per well). Phase contrast and dual-colour fluorescence images (excitation/emission settings; green 440–480/504–544 nm, red 565–605/625–705 nm, with spectral unmixing set as 8% of red removed from green) were collected for all experiments every 6 h for 7 days. The average live, dead (green fluorescence) and apoptotic (red fluorescence) cell count was determined from the replicated wells and data was expressed as mean (green or red) confluence per mm^2 ± SEM. The relative cell death and apoptosis was obtained by dividing the green or red fluorescence confluence area over the phase confluence area. The processing definitions for analyzing the confluences of phase and green and red fluorescence are described in Table S2.

Clonogenic cell survival assays

Cells were seeded into six-well plates at a density of 1,000 cells/well for OVSAHO and TYK-nu, and then treated with efavirenz (5.4–40 μM with 1.25-fold dilutions) for 14 days. For COV362, 500 cells/well were seeded into 6-well plates and treated with efavirenz for 9 days. After drug treatment, cells were fixed with 100% methanol for 20 min, rinsed briefly with water and stained with 0.25% w/v crystal violet in 25% v/v methanol for 5 min.[48] Colonies were counted using the GelCount imager (Oxford Optronix, Abingdon, England) and plating efficiency (PE) and surviving fraction (SF) determined.[49]

PARP activity assay

Levels of PARP1 enzyme activity in three HGSOC cell lines (COV362, OVSAHO, and TYK-nu) were measured using a PARP/Apoptosis Universal Colorimetric Assay (cat. #4677-096-K, R&D Systems, Minneapolis, MN, USA) as per the manufacturer's protocol. Briefly, cell pellets were collected after 72 h of treatment with efavirenz (25 μM, 35 μM, or 45 μM) or DMSO vehicle control, and the amount of protein was quantified using the Qubit Protein Assay Kit (cat. #33211, Thermo Fisher Scientific, MA, USA). Cell lysates containing 20 μg protein were loaded into histone-coated wells and incubated for an hour. Following further incubations with horseradish peroxidase conjugated streptavidin (strep-HRP) and the HRP substrate TACS-Sapphire, the reaction was stopped by adding 50 μL 0.2M HCl to each well and the plate was read at 450 nm with a microplate reader (BMG Labtech, Ortenberg, Germany).

Cell-cycle analysis

To determine the effect of efavirenz on cell-cycle distribution in studied cancer cells, a flow cytometry-based analysis was performed after staining the untreated and treated with 25, 35, or 45 μM efavirenz for 48 and 72 h, with propidium iodide (PI) solution. Briefly, 6×10^4 cells/well were seeded in 3 mL of medium per well in six-well plates. After overnight incubation at 37°C in 5% CO_2, the cells were incubated with efavirenz for specified time points. The medium-containing cells were then taken out from the wells and transferred to FACS tubes. Cells were then pelleted by centrifugation at 300 × *g* for 5 min. Afterward, cells were fixed by using 70% (v/v) ice-cold ethanol for 15 min and then again pelleted by centrifugation (300 × *g* for 5 min). Finally, the cells were incubated with 200 μL of PI staining solution (50 μg/mL PI, 0.1% sodium citrate, 0.1 mg/mL RNase A, and 0.1% Triton X-100) for 1.5 h at room temperature in the dark. After the incubation period, the cells were analyzed using a CytoFLEX flow cytometer (Beckman Coulter Inc., Brea, CA, USA). CytExpert software version 2.1 was used for data analysis and graph preparation.

Western blots

COV362, OVSAHO, and TYK-nu cells were treated with 25, 35, or 45 μM efavirenz for 48 and 72 h, and protein extracted using urea buffer as previously described.[45] Extracts were sonicated for 15 s followed by denaturation at 95°C for 5 min, and 7.5 μg of each sample was separated on a 4%–12% Bis-Tris gel (cat. #NP0336BOX, Life Technologies, Thornton, NSW, Australia) at 180 V for 1 h prior to being transferred to nitrocellulose membrane (cat. #10600016, Sigma-Aldrich, St. Louis, MO, United States) for 1.5 h using a wet transfer system (Bio-Rad, CA, United Sates). Nitrocellulose membranes were blocked with 50% (v/v) Intercept Blocking Buffer/TBS (cat. #927–60001, LI-COR Bioscience, Lincoln, NE, USA) and incubated overnight at 4°C with primary antibodies of interest. The

following primary antibodies were sourced from Thermofisher Scientific (Mulgrave, VIC, Australia): PARP1 (cat. #436400), PARP2 (cat. #MA5-38149), phospho-Histone H2A.X (Ser139) (cat. #MA1-2022) and CDK2 (cat. #MA5-17052). Further primary antibodies were sourced from Cell Signaling Technology (Danvers, MA, USA): phospho-RB (Ser780) (cat. #8180S) and GAPDH (14C10) (cat. #2118). Membranes were probed with the following appropriate species-specific near-infrared (NIR) fluorescent secondary antibodies: IRDye 800CW Donkey anti-Mouse IgG (cat. #LCR-926-32212) or IRDye 680RD Donkey anti-Rabbit (cat. #LCR-926-68073 from LI-COR Bioscience (Lincoln, NE, USA) for 1 h at room temperature and fluorescent signals visualized on the Odyssey CLx imaging system (LI-COR Bioscience, Lincoln, NE, USA). ImageStudio software version 5.2 (LI-COR Bioscience) was used for protein quantitation.

Statistical analysis

Statistical analyses were undertaken using IBM SPSS software version 28.0 (SPSS Australasia Pty Ltd., Chatswood, NSW, Australia). Results are expressed as the mean ± SEM from three replicate experiments. IncuCyte live-cell assay data was compared using a one-way ANOVA with Tukey's *post hoc* test for multiple comparisons between drug doses at 168 h in cell lines. PARP1 enzyme activity data were compared using a one-way ANOVA with Tukey's *post hoc* test for multiple comparisons between drug doses at 72 h in cell lines. Immunoblotting data were compared using a one-way ANOVA with Tukey's *post hoc* test for multiple comparisons within drug doses at either 48 or 72 h in cell lines. Differences were considered to be statistically significant when $p < 0.05$.

DATA AND CODE AVAILABILITY

The datasets analyzed during the current study (Figure S1) are available in the Broad Institute Repurposing Database (https://depmap.org/repurposing/).

All other data generated or analyzed during this study are included in this published article and its supplemental information files.

ACKNOWLEDGMENTS

This study was funded by the Australian Government Medical Research Future Fund Emerging Priorities and Consumer Driven Research Initiative (APP1199620), B.M. was funded by the Jill Emberson Memorial HMRI PhD scholarship and Tour de Cure and N.A.B. was funded by the Vanessa McGuigan Memorial HMRI Fellowship in Ovarian Cancer Research. Ms Tao Xie is acknowledged for genomic analyses of *BRCA2* levels in OVSAHO. We also acknowledge the contribution of ovarian cancer consumer Ms Gill Stannard in guiding the direction and priorities of the study.

AUTHOR CONTRIBUTIONS

B.M. and M.W.-B. collected, analyzed, and interpreted data and wrote the manuscript; D.L., C.Y., K.-A.D. collected and analyzed data and prepared figures for the manuscript; J.S. filtered and interpreted the BLAZE drug list, S.I. collected and analyzed the flow cytometry data and prepared the figure for the manuscript, R.H. and J.H.M. provided the BLAZE drug list and provided guidance in interpretation of the data, C.E.F. and D.J.M. supervised collection of data, analyzed and interpreted the data, N.A.B. co-ordinated the study, supervised collection and analysis of data, interpreted data, and collated the final version on the manuscript. All authors contributed to writing the manuscript.

DECLARATION OF INTERESTS

N.A.B. has received research funding from Merck KGaA and Bristol Myers Squibb (BMS) for investigator-initiated clinical trials not related to this study. J.S. has received funding from Becton, Dickinson and Company (BD) for research projects not related to this study. C.E.F. has received funding from Boehringer Ingelheim for research projects not related to this study. All other authors declare that they have no competing interests.

SUPPLEMENTAL INFORMATION

Supplemental information can be found online at https://doi.org/10.1016/j.omton.2024.200911.

REFERENCES

1. Sung, H., Ferlay, J., Siegel, R.L., Laversanne, M., Soerjomataram, I., Jemal, A., and Bray, F. (2021). Global Cancer Statistics 2020: GLOBOCAN Estimates of Incidence and Mortality Worldwide for 36 Cancers in 185 Countries. CA A Cancer J. Clin. *71*, 209–249. https://doi.org/10.3322/caac.21660.

2. Bowtell, D.D., Böhm, S., Ahmed, A.A., Aspuria, P.J., Bast, R.C., Jr., Beral, V., Berek, J.S., Birrer, M.J., Blagden, S., Bookman, M.A., et al. (2015). Rethinking ovarian cancer II: reducing mortality from high-grade serous ovarian cancer. Nat. Rev. Cancer *15*, 668–679. https://doi.org/10.1038/nrc4019.

3. Nosengo, N. (2016). Can you teach old drugs new tricks? Nature *534*, 314–316. https://doi.org/10.1038/534314a.

4. Ashburn, T.T., and Thor, K.B. (2004). Drug repositioning: identifying and developing new uses for existing drugs. Nat. Rev. Drug Discov. *3*, 673–683. https://doi.org/10.1038/nrd1468.

5. Pushpakom, S., Iorio, F., Eyers, P.A., Escott, K.J., Hopper, S., Wells, A., Doig, A., Guilliams, T., Latimer, J., McNamee, C., et al. (2019). Drug repurposing: progress, challenges and recommendations. Nat. Rev. Drug Discov. *18*, 41–58. https://doi.org/10.1038/nrd.2018.168.

6. Martin, J.H., and Bowden, N.A. (2020). Drug repurposing in the era of COVID-19: a call for leadership and government investment. Med. J. Aust. *212*, 450–452.e1. https://doi.org/10.5694/mja2.50603.

7. Zheng, F., Zhang, Y., Chen, S., Weng, X., Rao, Y., and Fang, H. (2020). Mechanism and current progress of Poly ADP-ribose polymerase (PARP) inhibitors in the treatment of ovarian cancer. Biomed. Pharmacother. *123*, 109661. https://doi.org/10.1016/j.biopha.2019.109661.

8. Rose, M., Burgess, J.T., O'Byrne, K., Richard, D.J., and Bolderson, E. (2020). PARP Inhibitors: Clinical Relevance, Mechanisms of Action and Tumor Resistance. Front. Cell Dev. Biol. *8*, 564601. https://doi.org/10.3389/fcell.2020.564601.

9. Helleday, T., Bryant, H.E., and Schultz, N. (2005). Poly(ADP-ribose) polymerase (PARP-1) in homologous recombination and as a target for cancer therapy. Cell Cycle *4*, 1176–1178. https://doi.org/10.4161/cc.4.9.2031.

10. Wong-Brown, M.W., van der Westhuizen, A., and Bowden, N.A. (2020). Targeting DNA Repair in Ovarian Cancer Treatment Resistance. Clin. Oncol. *32*, 518–526. https://doi.org/10.1016/j.clon.2020.03.005.

11. Xie, T., Dickson, K.A., Yee, C., Ma, Y., Ford, C.E., Bowden, N.A., and Marsh, D.J. (2022). Targeting Homologous Recombination Deficiency in Ovarian Cancer with PARP Inhibitors: Synthetic Lethal Strategies That Impact Overall Survival. Cancers *14*, 4621. https://doi.org/10.3390/cancers14194621.

12. Slade, D. (2019). Mitotic functions of poly(ADP-ribose) polymerases. Biochem. Pharmacol. *167*, 33–43. https://doi.org/10.1016/j.bcp.2019.03.028.

13. Weaver, A.N., and Yang, E.S. (2013). Beyond DNA Repair: Additional Functions of PARP-1 in Cancer. Front. Oncol. *3*, 290. https://doi.org/10.3389/fonc.2013.00290.

14. Marima, R., Hull, R., Dlamini, Z., and Penny, C. (2020). Efavirenz induces DNA damage response pathway in lung cancer. Oncotarget *11*, 3737–3748. https://doi.org/10.18632/oncotarget.27725.

15. Marima, R., Hull, R., Dlamini, Z., and Penny, C. (2020). Efavirenz and Lopinavir/Ritonavir Alter Cell Cycle Regulation in Lung Cancer. Front. Oncol. *10*, 1693. https://doi.org/10.3389/fonc.2020.01693.

16. Bruning, A., Juckstock, J., Kost, B., Tsikouras, P., Weissenbacher, T., Mahner, S., and Mylonas, I. (2017). Induction of DNA damage and apoptosis in human leukemia cells by efavirenz. Oncol. Rep. *37*, 617–621. https://doi.org/10.3892/or.2016.5243.

17. Sikora, M.J., Rae, J.M., Johnson, M.D., and Desta, Z. (2010). Efavirenz directly modulates the oestrogen receptor and induces breast cancer cell growth. HIV Med. *11*, 603–607. https://doi.org/10.1111/j.1468-1293.2010.00831.x.

18. Chiou, P.T., Ohms, S., Board, P.G., Dahlstrom, J.E., Rangasamy, D., and Casarotto, M.G. (2021). The Antiviral Drug Efavirenz in Breast Cancer Stem Cell Therapy. Cancers *13*, 6232. https://doi.org/10.3390/cancers13246232.

19. Chiou, P.T., Ohms, S., Board, P.G., Dahlstrom, J.E., Rangasamy, D., and Casarotto, M.G. (2021). Efavirenz as a potential drug for the treatment of triple-negative breast cancers. Clin. Transl. Oncol. *23*, 353–363. https://doi.org/10.1007/s12094-020-02424-5.

20. Hecht, M., Erber, S., Harrer, T., Klinker, H., Roth, T., Parsch, H., Fiebig, N., Fietkau, R., and Distel, L.V. (2015). Efavirenz Has the Highest Anti-Proliferative Effect of Non-Nucleoside Reverse Transcriptase Inhibitors against Pancreatic Cancer Cells. PLoS One *10*, e0130277. https://doi.org/10.1371/journal.pone.0130277.

21. Hecht, M., Harrer, T., Körber, V., Sarpong, E.O., Moser, F., Fiebig, N., Schwegler, M., Stürzl, M., Fietkau, R., and Distel, L.V. (2018). Cytotoxic effect of Efavirenz in BxPC-3 pancreatic cancer cells is based on oxidative stress and is synergistic with ionizing radiation. Oncol. Lett. *15*, 1728–1736. https://doi.org/10.3892/ol.2017.7523.

22. Han, M., Wang, S., Yang, N., Wang, X., Zhao, W., Saed, H.S., Daubon, T., Huang, B., Chen, A., Li, G., et al. (2020). Therapeutic implications of altered cholesterol homeostasis mediated by loss of CYP46A1 in human glioblastoma. EMBO Mol. Med. *12*, e10924. https://doi.org/10.15252/emmm.201910924.

23. Perna, A., Lucariello, A., Sellitto, C., Agliata, I., Carleo, M.A., Sangiovanni, V., Esposito, V., Guerra, G., Cobellis, L., and De Luca, A. (2017). Different Cell Cycle Modulation in SKOV-3 Ovarian Cancer Cell Line by Anti-HIV Drugs. Oncol. Res. *25*, 1617–1624. https://doi.org/10.3727/096504017X14905635363102.

24. Houede, N., Pulido, M., Mourey, L., Joly, F., Ferrero, J.M., Bellera, C., Priou, F., Lalet, C., Laroche-Clary, A., Raffin, M.C., et al. (2014). A phase II trial evaluating the efficacy and safety of efavirenz in metastatic castration-resistant prostate cancer. Oncologist *19*, 1227–1228. https://doi.org/10.1634/theoncologist.2014-0345.

25. Griffiths, C.T., Hall, T.C., Saba, Z., Barlow, J.J., and Nevinny, H.B. (1973). Preliminary trial of aminoglutethimide in breast cancer. Cancer *32*, 31–37. https://doi.org/10.1002/1097-0142(197307)32:1<31::aid-cncr2820320104>3.0.co;2-5.

26. Strategies for Management of Anti-Retroviral Therapy/INSIGHT; DAD Study Groups (2008). Use of nucleoside reverse transcriptase inhibitors and risk of myocardial infarction in HIV-infected patients. AIDS *22*, F17–F24. https://doi.org/10.1097/QAD.0b013e32830fe35e.

27. Therapeutic Goods Administration (2018). Ganciclovir SXP (ganciclovir). https://www.ebs.tga.gov.au/ebs/picmi/picmirepository.nsf/pdf?OpenAgent=&id=CP-2017-PI-02645-1&d=20230826172310101.

28. Lukasik, P., Zaluski, M., and Gutowska, I. (2021). Cyclin-Dependent Kinases (CDK) and Their Role in Diseases Development-Review. Int. J. Mol. Sci. *22*, 2935. https://doi.org/10.3390/ijms22062935.

29. Domcke, S., Sinha, R., Levine, D.A., Sander, C., and Schultz, N. (2013). Evaluating cell lines as tumour models by comparison of genomic profiles. Nat. Commun. *4*, 2126. https://doi.org/10.1038/ncomms3126.

30. Vrouenraets, S.M.E., Wit, F.W.N.M., van Tongeren, J., and Lange, J.M.A. (2007). Efavirenz: a review. Expet Opin. Pharmacother. *8*, 851–871. https://doi.org/10.1517/14656566.8.6.851.

31. Deeks, E.D., and Perry, C.M. (2010). Efavirenz/emtricitabine/tenofovir disoproxil fumarate single-tablet regimen (Atripla(R)): a review of its use in the management of HIV infection. Drugs *70*, 2315–2338. https://doi.org/10.2165/11203800-000000000-00000.

32. Therapeutic Goods Administration (2023). STOCRIN® (efavirenz) Tablets. https://www.ebs.tga.gov.au/ebs/picmi/picmirepository.nsf/pdf?OpenAgent=&id=CP-2010-PI-01181-3.

33. Faltz, M., Bergin, H., Pilavachi, E., Grimwade, G., and Mabley, J.G. (2017). Effect of the Anti-retroviral Drugs Efavirenz, Tenofovir and Emtricitabine on Endothelial Cell Function: Role of PARP. Cardiovasc. Toxicol. *17*, 393–404. https://doi.org/10.1007/s12012-016-9397-4.

34. Rouleau, M., Patel, A., Hendzel, M.J., Kaufmann, S.H., and Poirier, G.G. (2010). PARP inhibition: PARP1 and beyond. Nat. Rev. Cancer *10*, 293–301. https://doi.org/10.1038/nrc2812.

35. Menear, K.A., Adcock, C., Boulter, R., Cockcroft, X.L., Copsey, L., Cranston, A., Dillon, K.J., Drzewiecki, J., Garman, S., Gomez, S., et al. (2008). 4-[3-(4-cyclopropanecarbonylpiperazine-1-carbonyl)-4-fluorobenzyl]-2H-phthalazin-1-one: a novel bioavailable inhibitor of poly(ADP-ribose) polymerase-1. J. Med. Chem. *51*, 6581–6591. https://doi.org/10.1021/jm8001263.

36. Thomas, H.D., Calabrese, C.R., Batey, M.A., Canan, S., Hostomsky, Z., Kyle, S., Maegley, K.A., Newell, D.R., Skalitzky, D., Wang, L.Z., et al. (2007). Preclinical selection of a novel poly(ADP-ribose) polymerase inhibitor for clinical trial. Mol. Cancer Therapeut. *6*, 945–956. https://doi.org/10.1158/1535-7163.MCT-06-0552.

37. Jones, P., Altamura, S., Boueres, J., Ferrigno, F., Fonsi, M., Giomini, C., Lamartina, S., Monteagudo, E., Ontoria, J.M., Orsale, M.V., et al. (2009). Discovery of 2-4-[(3S)-piperidin-3-yl]phenyl-2H-indazole-7-carboxamide (MK-4827): a novel oral poly(ADP-ribose)polymerase (PARP) inhibitor efficacious in BRCA-1 and -2 mutant tumors. J. Med. Chem. *52*, 7170–7185. https://doi.org/10.1021/jm901188v.

38. Hecht, M., Harrer, T., Büttner, M., Schwegler, M., Erber, S., Fietkau, R., and Distel, L.V. (2013). Cytotoxic effect of efavirenz is selective against cancer cells and associated with the cannabinoid system. AIDS *27*, 2031–2040. https://doi.org/10.1097/QAD.0b013e3283625444.

39. Staszewski, S., Morales-Ramirez, J., Tashima, K.T., Rachlis, A., Skiest, D., Stanford, J., Stryker, R., Johnson, P., Labriola, D.F., Farina, D., et al. (1999). Efavirenz plus zidovudine and lamivudine, efavirenz plus indinavir, and indinavir plus zidovudine and lamivudine in the treatment of HIV-1 infection in adults. Study 006 Team. N. Engl. J. Med. *341*, 1865–1873. https://doi.org/10.1056/NEJM199912163412501.

40. Albrecht, M.A., Bosch, R.J., Hammer, S.M., Liou, S.H., Kessler, H., Para, M.F., Eron, J., Valdez, H., Dehlinger, M., and Katzenstein, D.A.; AIDS Clinical Trials Group 364 Study Team (2001). Nelfinavir, efavirenz, or both after the failure of nucleoside treatment of HIV infection. N. Engl. J. Med. *345*, 398–407. https://doi.org/10.1056/NEJM200108093450602.

41. Cheeseright, T.J., Mackey, M.D., Melville, J.L., and Vinter, J.G. (2008). FieldScreen: virtual screening using molecular fields. Application to the DUD data set. J. Chem. Inf. Model. *48*, 2108–2117. https://doi.org/10.1021/ci800110p.

42. Corsello, S.M., Nagari, R.T., Spangler, R.D., Rossen, J., Kocak, M., Bryan, J.G., Humeidi, R., Peck, D., Wu, X., Tang, A.A., et al. (2020). Discovering the anti-cancer potential of non-oncology drugs by systematic viability profiling. Nat. Can. (Ott.) *1*, 235–248. https://doi.org/10.1038/s43018-019-0018-6.

43. Coscia, F., Watters, K.M., Curtis, M., Eckert, M.A., Chiang, C.Y., Tyanova, S., Montag, A., Lastra, R.R., Lengyel, E., and Mann, M. (2016). Integrative proteomic profiling of ovarian cancer cell lines reveals precursor cell associated proteins and functional status. Nat. Commun. *7*, 12645. https://doi.org/10.1038/ncomms12645.

44. Beaufort, C.M., Helmijr, J.C.A., Piskorz, A.M., Hoogstraat, M., Ruigrok-Ritstier, K., Besselink, N., Murtaza, M., van IJcken, W.F.J., Heine, A.A.J., Smid, M., et al. (2014). Ovarian cancer cell line panel (OCCP): clinical importance of in vitro morphological subtypes. PLoS One *9*, e103988. https://doi.org/10.1371/journal.pone.0103988.

45. Dickson, K.A., Xie, T., Evenhuis, C., Ma, Y., and Marsh, D.J. (2021). PARP Inhibitors Display Differential Efficacy in Models of BRCA Mutant High-Grade Serous Ovarian Cancer. Int. J. Mol. Sci. *22*, 8506. https://doi.org/10.3390/ijms22168506.

46. Werner, B., Yuwono, N., Duggan, J., Liu, D., David, C., Srirangan, S., Provan, P., INOVATe Investigators, DeFazio, A., Arora, V., et al. (2021). Cell-free DNA is abundant in ascites and represents a liquid biopsy of ovarian cancer. Gynecol. Oncol. *162*, 720–727. https://doi.org/10.1016/j.ygyno.2021.06.028.

47. Sebaugh, J.L. (2011). Guidelines for accurate EC50/IC50 estimation. Pharmaceut. Stat. *10*, 128–134. https://doi.org/10.1002/pst.426.

48. Crowley, L.C., Christensen, M.E., and Waterhouse, N.J. (2016). Measuring Survival of Adherent Cells with the Colony-Forming Assay. Cold Spring Harb. Protoc. *2016*. https://doi.org/10.1101/pdb.prot087171.

49. Unkel, S., Belka, C., and Lauber, K. (2016). On the analysis of clonogenic survival data: Statistical alternatives to the linear-quadratic model. Radiat. Oncol. *11*, 11. https://doi.org/10.1186/s13014-016-0584-z.